

# Combining quantum noise reduction resources: a practical approach

Sohitri Ghosh<sup>a,b,\*</sup>, Matthew A. Feldman<sup>c,d,†</sup>, Seongjin Hong<sup>c,d</sup>,  
 Claire Marvinney<sup>c,d</sup>, Raphael Pooser<sup>c,d</sup>, and Jacob M. Taylor<sup>a,b,‡</sup>

<sup>a</sup> *Joint Quantum Institute/Joint Center for Quantum Information and Computer Science,  
 University of Maryland, College Park/National Institute of Standards and Technology, Gaithersburg, MD, USA*

<sup>b</sup> *Department of Physics, University of Maryland, College Park, MD, USA*

<sup>c</sup> *Quantum Information Science Section, Oak Ridge National Laboratory, Oak Ridge, TN 37831, USA and*

<sup>d</sup> *Quantum Science Center, Oak Ridge National Laboratory, Oak Ridge, TN 37831, USA*

(Dated: November 29, 2022)

Optomechanical sensors are capable of transducing external perturbations to resolvable optical signals. A particular regime of interest is that of high-bandwidth force detection, where an impulse is delivered to the system over a short period of time. Exceedingly sensitive impulse detection has been proposed to observe very weak signals like those for long range interactions with dark matter requiring much higher sensitivities than current sensors can provide. Quantum resources to go beyond the standard quantum limit of noise in these sensors include squeezing of the light used to transduce the signal, backaction evasion by measuring the optimum quadrature, and quantum non-demolition (QND) measurements which reduce backaction directly. However, it has been extremely difficult to determine a scheme where all these quantum resources contribute to noise reduction thereby exceeding the benefit of using only one quantum resource alone. We provide the theoretical limits to noise reduction while combining quantum enhanced readout techniques such as squeezing and QND measurements for these optomechanical sensors. We demonstrate that backaction evasion through QND techniques dramatically reduces the technical challenges presented when using squeezed light for broadband force detection, paving the way for combining multiple quantum noise reduction techniques for enhanced sensitivity in the context of impulse metrology.

## I. INTRODUCTION

State-of-the-art force sensors operate near the standard quantum limit (SQL) making possible the detection of weak impulses relevant to a plethora of physics [1–5]. Broadband impulse metrology has recently been proposed to detect dark matter [6–8] and involves the measurement of rapid and minute impulses allowing for the detection of forces across a wide range of frequencies. Currently, the Windchime collaboration is developing such impulse measurement techniques using an array of mechanical sensors to aim for heavy dark matter detection through long range interactions [9]. Impulse metrology has potential applications in other fields as well including but not limited to low-energy single-photon detection and quantum noise-limited pressure calibrations accounting for gas collisions [10–14]. We are interested in impulse metrology with optomechanical sensors. Op-

tomechanical sensors work by transducing a force acting on mechanical systems to measurable optical signals and are relevant to very sensitive force measurements [15–20].

Squeezed light and backaction evasion (BAE) are quantum resources that may be leveraged to reduce the measurement-induced noise below the SQL. Squeezed light has been used to enhance the signal-to-noise ratio (SNR) in atomic-force microscopy [21] and micro-electromechanical (MEMS) cantilevers [22], and most famously to detect gravitational waves in the LIGO collaboration [23]. However, in traditional quantum enhanced metrology, position measurements with squeezed light have the maximum benefit when realized for a narrow-band force signal [24, 25]. We also consider quantum non-demolition (QND) measurements, where repeated measurements of a single observable result in no increment in uncertainty over time and yield the same precise result every time in the absence of any external influence. A QND measurement is accomplished when an observable is unaffected due to the quantum uncertainty produced in the corresponding non-commutative conjugate variable [1, 26–28]. A class of QND measurements known as backaction evading measurements are attainable when we can measure an observable devoid of backaction from the measuring apparatus. Backaction evasion experiments have been implemented using four-wave mixing [29] and optical parametric amplifiers [30], and have enhanced the sensitivity of optomechanical systems [31–35]. Several quantum noise reduction techniques have been investigated especially in the context of gravitational wave [36–40] and dark matter detection [41–44]. Here, we will focus on the prospect of using squeezing, backaction evasion and QND techniques simultaneously to enhance sensitiv-

\* sohitri@umd.edu ; Notice: This manuscript has been authored by UT-Battelle, LLC, under contract DE-AC05-00OR22725 with the US Department of Energy (DOE). The US government retains and the publisher, by accepting the article for publication, acknowledges that the US government retains a nonexclusive, paid-up, irrevocable, worldwide license to publish or reproduce the published form of this manuscript, or allow others to do so, for US government purposes. DOE will provide public access to these results of federally sponsored research in accordance with the DOE Public Access Plan (<http://energy.gov/downloads/doe-public-access-plan>).

† feldmanma@ornl.gov

‡ jmtaylor@umd.edu ; current address Riverlane Research, Inc., One Broadway, Cambridge MA 02139

ity to weak impulses.

In this article, we determine the advantages of probing optomechanical systems with squeezed light in position and momentum sensing schemes combining two different quantum noise reduction methods. We find that the noise reduction through squeezing is compatible with the concurrent implementation of backaction evasion through a QND momentum measurement in the free mass regime. Our noise reduction scheme has implications to dark matter detection and quantum metrology more broadly, as our scheme provides an improvement over a broad frequency band and simultaneously simplifies the technical challenges of using squeezed light for impulse metrology.

We first introduce a toy model to illustrate the advantages of position measurements using single- and two-mode squeezed light. The expected losses and asymmetry in displacement amplitude are characterized for the single- and two-mode cases, respectively. Our scheme is shown to be robust against small amounts of loss and displacement amplitude asymmetries. Second, we examine a specific interferometric optomechanical system and find that, in principle, BAE and squeezing can be combined over a broad bandwidth when reading out the momentum. Our results show that squeezed momentum measurements facilitate broadband impulse metrology with quantum-enhanced sensitivity in the parameter regimes required for dark matter detection.

## II. BENEFITS OF SQUEEZING

### A. Single-mode Squeezing Toy Model

Here, we present a toy model for a backaction induced measurement system, where light interacts with the position of the system twice, and the interactions are separated by the free evolution of the system in between, as seen in the schematic diagram of Fig. 1a and the proposed experimental implementation of Fig. 3a. The interaction Hamiltonian for our toy model is given by

$$H_{\text{int}} = \hbar G x X, \quad (1)$$

where  $x$  is the position of the system,  $X$  is the amplitude quadrature of light, and  $G$  is the optomechanical coupling strength enhanced by the displacement amplitude  $\alpha$ . A full description of the dependence of this interaction on the displacement amplitude is provided in appendix A. In our model, the radiation pressure of the light alters the momentum of the mechanical system. During the free evolution of the system, this shift in momentum causes a change in the position of the optomechanical system as seen in Fig. 1a. Incorporating the free evolution in this manner allows us to model the effect of the backaction in the system. In the subsequent interaction, the change in position is transduced to the phase quadrature of the

light,  $Y$ . The above has following unitary evolution:

$$U_{\text{tot}} = U_{\text{int}} U_{\text{free}} U_{\text{int}} = e^{-i\zeta x_0 X} e^{-i\beta \frac{p_0^2}{2}} e^{-i\zeta x_0 X}, \quad (2)$$

where  $x_0$  and  $p_0$  are the dimensionless position and momentum operators of the optomechanical system. These are normalized to a length and momentum scale comparable to the De Broglie wavelength  $\lambda = \sqrt{\frac{\hbar^2}{2mK_B T}}$  where  $m$  and  $T$  are the mass and temperature of the moving mirror, respectively. For a harmonic oscillator scenario, the length scale is set by  $K_B T \rightarrow \hbar\omega$ . We note that the more common continuous process is approximated by our toy model as it represents the third-order Suzuki-Trotter approximation. Thus, we interpret the parameter  $\beta$  as a dimensionless factor accounting for the free evolution of the system described by  $\beta = \hbar t / (m\lambda^2)$  with the free evolution time  $t \sim 1/\kappa$  where  $\kappa$  is the cavity linewidth. The parameter  $\zeta$  is dependent on the displacement amplitude of the optical pulse via,  $\zeta = \alpha\mu$ , where  $\mu$  is a dimensionless quantity defined in terms of the interaction time and the single photon optomechanical coupling strength in frequency units  $g$ ,  $\mu \sim g/\kappa$ . As shown in the appendix A, we find that existing optomechanical systems have sufficient single-photon optomechanical coupling strengths and cavity linewidths for our interaction Hamiltonian to be valid [45, 46]. By applying these unitaries, the momentum, the phase quadrature of the probing light and the position operators transform as follows,

$$\begin{aligned} U_{\text{int}}^\dagger p_0 U_{\text{int}} &= p_0 - \zeta X, \\ U_{\text{int}}^\dagger Y U_{\text{int}} &= Y - \zeta x_0, \text{ and} \\ U_{\text{free}}^\dagger x_0 U_{\text{free}} &= x_0 + \beta p_0. \end{aligned} \quad (3)$$

The remaining unitary transformations do not change the operators since  $X$ ,  $Y$  and  $p_0$  commute with  $U_{\text{free}}$  and  $x_0$  and  $X$  commute with  $U_{\text{int}}$ . The transformation of the operators under the full unitary evolution Eq. 2 can be represented as,

$$\begin{aligned} Y' &= U_{\text{tot}}^\dagger Y U_{\text{tot}} = Y - 2\zeta x_0 - \zeta\beta p_0 + \zeta^2\beta X, \\ X' &= U_{\text{tot}}^\dagger X U_{\text{tot}} = X, \\ x' &= U_{\text{tot}}^\dagger x U_{\text{tot}} = x_0 + \beta p_0 - \beta\zeta X, \\ p' &= U_{\text{tot}}^\dagger p U_{\text{tot}} = p_0 - 2\zeta X. \end{aligned} \quad (4)$$

Let us consider the arbitrary quadrature  $X_\theta$  output from the system described by the unitary transformations in Eq. 4

$$\begin{aligned} X_\theta &= Y' \cos \theta + X' \sin \theta \\ &= \cos \theta (Y - 2\zeta x_0 - \zeta\beta p_0 + \zeta^2\beta X) + \sin \theta X, \end{aligned} \quad (5)$$

where  $X'$  and  $Y'$  are the output amplitude and phase quadratures of the system (see Fig. 1a), and  $\theta$  is the quadrature angle. We see that the quadrature has shot noise terms independent of  $\zeta$ , signal terms proportional

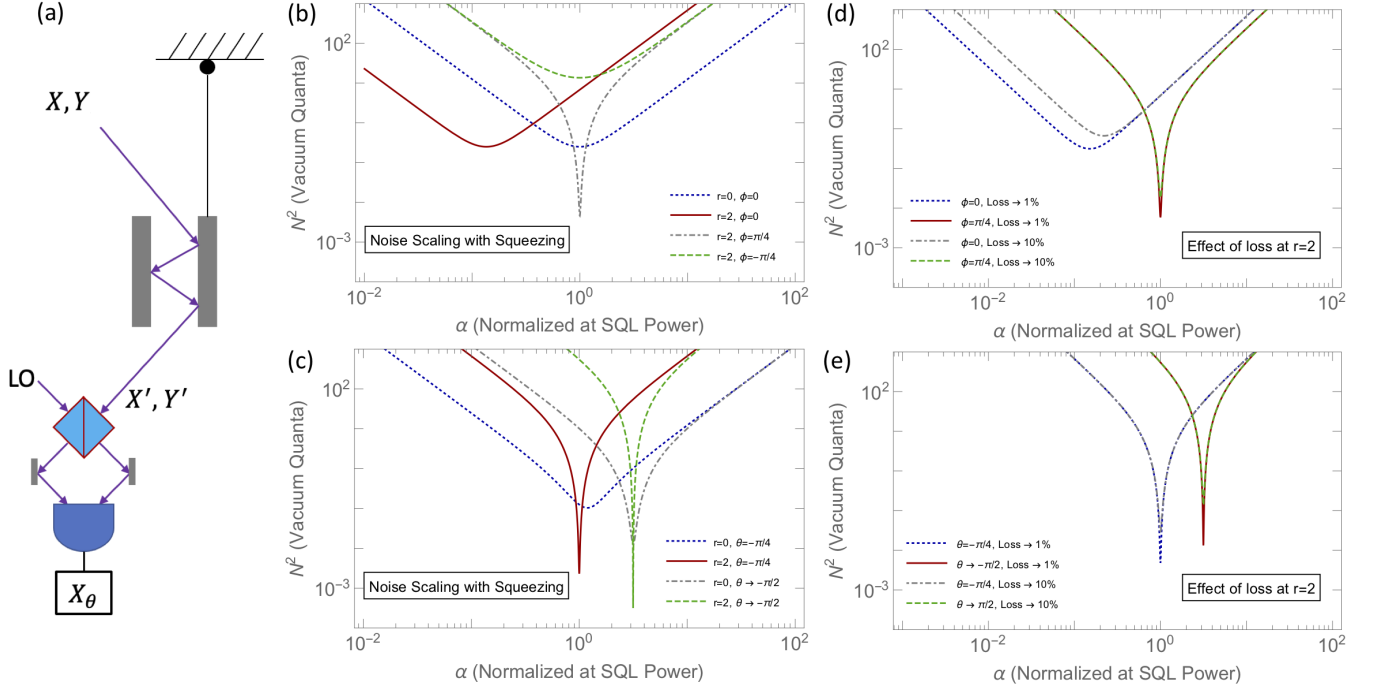


Figure 1. Position measurements using single-mode squeezed light. a) A position measurement comprising a single-sided optomechanical system probed with single-mode squeezed light with quadratures  $X$  and  $Y$ . In this proposed scheme the measured quadrature  $X_\theta$  is read out using homodyne detection by interfering the output with a local oscillator (LO). b) Phase quadrature measurement ( $\theta = 0$ ) at squeezing strengths  $r = 0, 2$  and squeezing angles  $\phi = 0, \pm\pi/4$  with the parameter  $\beta = 1$ . The displacement amplitude  $\alpha$  is normalized to the power required to achieve the SQL. Here the power at the SQL is the solution to Eq. 7 where we optimize with respect to  $\alpha$  at  $\theta, \phi = 0$ . The optimal noise floor for measuring the phase quadrature with  $r > 0$  occurs at  $\phi = \pi/4$  while at  $\phi = 0$  squeezing provides a reduced power to attain the same noise floor. c) Noise for measurement quadratures  $\theta = -\pi/4, -\pi/2$  with  $\phi = 0$  and  $\beta = 1$  where the optimal noise floor occurs at a  $\theta = -\pi/2$ , effectively an amplitude quadrature measurement. d) Effect of loss on phase quadrature measurement. e) Effect of loss on quadrature measurements  $\theta = -\pi/4, -\pi/2$ .

to  $\zeta$  and a backaction term proportional to  $\zeta^2$ . For the right combination of quadratures, the  $\sin\theta X$  term can cancel the backaction term. Another way to reduce the backaction noise is through quantum non-demolition measurements [26]. In this scenario, we can continuously monitor a QND variable like momentum in a free particle system instead of the position, to reduce or eliminate the backaction term, thereby achieving backaction evasion. In section IV we discuss how to perform a QND measurement to evade backaction noise in detail. For the toy model, we restrict our discussion to the continuous monitoring of position to showcase the benefits of squeezing. We obtain the estimator variable  $x_E$  for the system position by dividing  $X_\theta$  by the multiplicative factor  $2\zeta \cos\theta$ ,

$$x_E = X_\theta / (-2\zeta \cos\theta) = -\frac{Y}{2\zeta} + x_0 + \frac{\beta p_0}{2} - \frac{\zeta \beta X}{2} - \frac{\tan\theta X}{2\zeta}. \quad (6)$$

From Eq. 6, we see that a judicious choice of  $\theta$  allows us to cancel out the backaction noise from the amplitude quadrature. We find that the optimal  $\theta$  is dependent on  $\zeta^2$  (which is proportional to power  $\alpha^2$ ). The noise power spectral density (PSD) is proportional to the square of

the estimator variable,  $x_E$ . To analyze the measurement-induced noise of our system we evaluate  $N^2 = (x_E - (x_0 + \beta p_0/2))^2$ , since  $N^2$  is proportional to the variance of the system position, which may be written as

$$N^2 = \frac{Y^2}{4\zeta^2} + \frac{\zeta^2 \beta^2 X^2}{4} + \frac{\tan^2\theta X^2}{4\zeta^2} + \frac{\beta\{X, Y\}}{4} + \frac{\tan\theta\{X, Y\}}{4\zeta^2} + \frac{\beta \tan\theta X^2}{2}. \quad (7)$$

For squeezed light all of the terms in Eq. 7 are non-zero. The vacuum expectation values of the correlators after squeezing can be represented as [47],

$$\begin{aligned} \langle X^2 \rangle &= \frac{1}{2} (e^{2r} \cos^2\phi + e^{-2r} \sin^2\phi), \\ \langle Y^2 \rangle &= \frac{1}{2} (e^{-2r} \cos^2\phi + e^{2r} \sin^2\phi), \text{ and} \\ \langle \{X, Y\} \rangle &= \frac{1}{2} (e^{-2r} - e^{2r}) \sin 2\phi, \end{aligned} \quad (8)$$

where  $r, \phi$  are the squeezing strength and squeezing angle, respectively. For a position measurement, where

the phase quadrature ( $\theta \rightarrow 0$ ) is measured, the cross-correlator term can be made negative by choosing a suitable squeezing angle and increasing the squeezing strength to reduce the noise floor,  $N^2$  as seen in Fig. 1b. We can access the same noise floor at a lower power by probing the system with squeezed light (red solid curve) rather than a coherent state (blue dashed curve). A squeezing angle of  $\phi = \pi/4$  provides a lower noise floor (gray dashed curve) at the original power. This scenario is attained by adding a negative contribution from the cross-correlator term to the noise.

Alternatively, we explore combinations of the quadratures which reduces the backaction term to achieve a lower noise floor when using squeezed light (see Fig. 1c). We may globally minimize the contribution of the measurement-induced noise by optimizing the quadrature angle  $\theta$ . The optimization at  $\phi = 0$  gives us

$$\theta \rightarrow -\tan^{-1}(\zeta^2 \beta). \quad (9)$$

Here, we see that the quadrature angle is strongly dependent on the power of the light. Hence, when working deep in the backaction limit, at high power we are nearly measuring the amplitude quadrature which is devoid of any information about the system position, and slight fluctuation in power will destroy this benefit.

The optical losses in our system are a critical consideration when probing it with squeezed light. Here, we evaluate the effect of the expected optical losses of our system on the noise floor. For an overcoupled cavity where the intrinsic losses through any channel other than the input port are negligible, the cavity losses would approximately be of the same order as the loss at the detection port. Thus here, we investigate only the effects of the loss at the detection port. We determine the effect of adding vacuum noise at the output port of the beamsplitter used in homodyne detection. This can be represented by the following phase and amplitude measurement output,

$$\begin{aligned} Y_{\text{out}} &= Y' \cos(\eta) + Y'_{\text{in}} \sin(\eta), \text{ and} \\ X_{\text{out}} &= X' \cos(\eta) + X'_{\text{in}} \sin(\eta) \end{aligned} \quad (10)$$

where  $\eta^2$  quantifies the loss percentage in the system. Here  $Y'_{\text{in}}$  and  $X'_{\text{in}}$  are the input vacuum noise quadratures. We now focus on measuring the combination of the modified output phase and amplitude quadratures

$$X_{\theta, \text{out}} = Y_{\text{out}} \cos \theta + X_{\text{out}} \sin \theta. \quad (11)$$

By applying the same noise analysis as in the previous section, we demonstrate that the benefits of squeezing persist even at optical losses expected in experiments (see Fig. 1d-e).

## B. Two-mode Squeezing Toy Model

In this section, we consider using two-mode squeezed light to continuously monitor the position of an op-

tomechanical system. We find that for an approximate two-mode interaction, all the benefits expected from the single-mode case can be realized. Our system comprises a two-sided optical cavity with a pendulous mirror centered between two fixed mirrors as seen in the schematic diagram of Fig. 2a and the proposed experimental implementation of Fig. 3b. When the two modes are incident on opposite sides of the pendulous mirror with equal power, the interaction Hamiltonian is

$$H_{\text{int}} = \hbar G x(X_1 - X_2), \quad (12)$$

where  $X_i$  is the amplitude quadrature of light for the  $i^{\text{th}}$  mode. We now evaluate a toy model where two modes drive our backaction induced measurement system. In a manner analogous to the single-mode case, these dynamics can be characterized by applying the following chain of unitaries to the system,

$$U_{\text{int}} U_{\text{free}} U_{\text{int}} = e^{-i\zeta x_0(X_1 - X_2)} e^{-i\beta \frac{p_0^2}{2}} e^{-i\zeta x_0(X_1 - X_2)}. \quad (13)$$

Consequently, the following operators transform to,

$$\begin{aligned} U_{\text{int}}^\dagger p_0 U_{\text{int}} &= p_0 - \zeta(X_1 - X_2), \\ U_{\text{int}}^\dagger Y_1 U_{\text{int}} &= Y_1 - \zeta x_0, \\ U_{\text{int}}^\dagger Y_2 U_{\text{int}} &= Y_2 + \zeta x_0, \text{ and} \\ U_{\text{free}}^\dagger x_0 U_{\text{free}} &= x_0 + \beta p_0. \end{aligned} \quad (14)$$

Similar to the single-mode case, the remaining transformations do not change the operators since  $X_i$ ,  $Y_i$ , and  $p_0$  commute with  $U_{\text{free}}$  and  $x_0$ , and  $X_i$  commute with  $U_{\text{int}}$ . Under standard homodyne detection schemes, we have access to sums or differences of the quadratures,  $X_i$  and  $Y_i$  where  $i$  denotes the modes. We consider the arbitrary combination of differences in the  $X'_i$  and  $Y'_i$  quadratures between the output modes

$$\begin{aligned} X_\theta &= \cos \theta (Y'_1 - Y'_2) + \sin \theta (X'_1 - X'_2), \\ &= (\Delta Y - 4\zeta x_0 - 2\zeta \beta p_0 + 2\zeta^2 \beta \Delta X) \cos \theta + \Delta X \sin \theta, \end{aligned} \quad (15)$$

where  $\Delta Y = Y_1 - Y_2$  and  $\Delta X = X_1 - X_2$  are the phase difference quadrature and amplitude difference quadrature, respectively. Similar to the single-mode case, we find shot noise terms independent of  $\zeta$ , signal terms proportional to  $\zeta$  and backaction term proportional to  $\zeta^2$ . The estimator variable for measuring the position can be obtained by dividing the above quadrature through the multiplicative factor of  $x_0$  in Eq. 15,

$$\begin{aligned} x_E &= X_\theta / (-4\zeta \cos \theta) \\ &= -\frac{1}{4\zeta} \Delta Y + x_0 + \frac{\beta p_0}{2} - \frac{\zeta \beta}{2} \Delta X - \frac{\tan \theta}{4\zeta} \Delta X. \end{aligned} \quad (16)$$

As in the single-mode case, we only consider the measurement-induced noise terms from the light quadratures. Yet again, we can select a  $\theta$  in Eq. 16, to negate

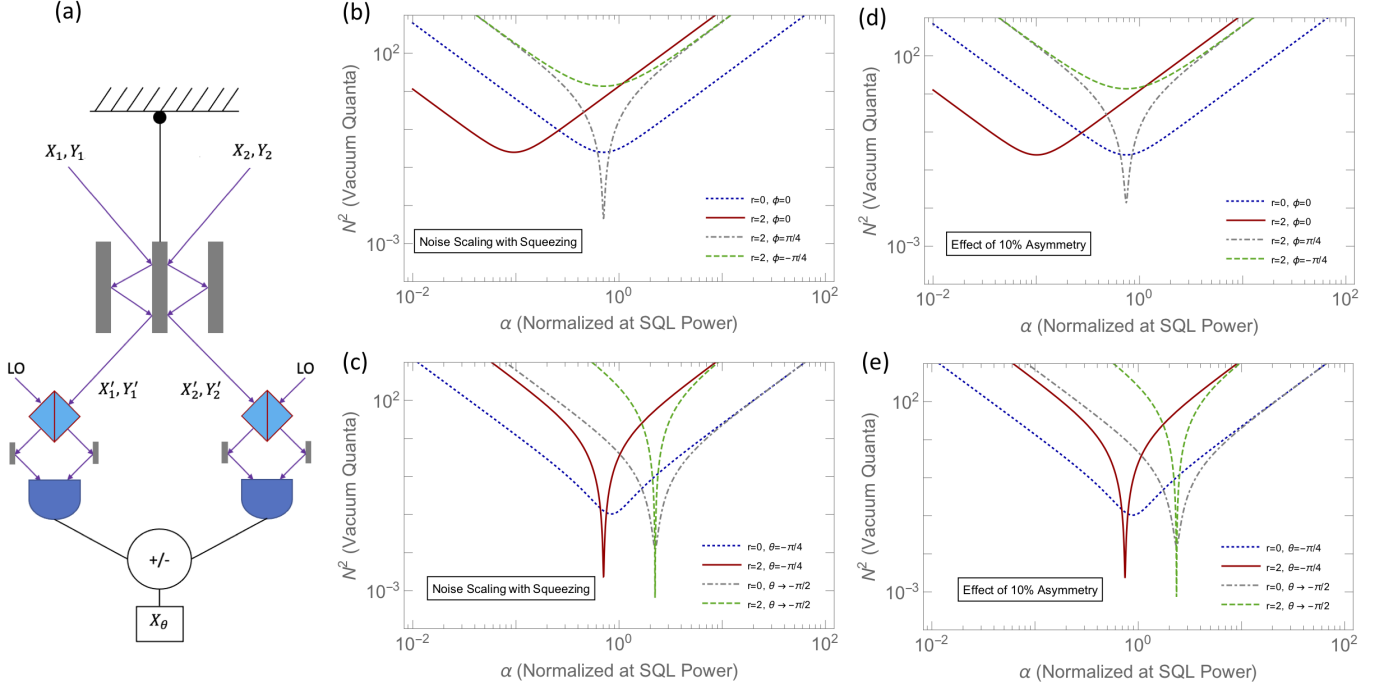


Figure 2. Position measurements using two-mode squeezed light. a) A position measurement comprising a two-sided optomechanical system probed with two-mode squeezed light with quadratures  $X_1, X_2$  and  $Y_1, Y_2$ . In this proposed scheme the measured quadrature  $X_\theta$  is read out using homodyne detection by interfering the outputs with their local oscillators (LO). b) Phase difference quadrature measurement ( $\theta = 0$ ) at squeezing strengths  $r = 0, 2$  and squeezing angles  $\phi = 0, \pm\pi/4$ . The displacement amplitude  $\alpha$  is normalized at the power required to reach the SQL for the single-mode (in Fig 1) for comparison. The optimal noise floor for measuring the phase difference quadrature with  $r > 0$  occurs at  $\phi = \pi/4$ , while at  $\phi = 0$  squeezing provides a reduced power to attain the same noise floor. c) Noise for measurement quadratures  $\theta = -\pi/4, -\pi/2$  where the optimal noise floor occurs at  $\theta = -\pi/2$ , effectively an amplitude difference quadrature measurement. d) Effect on phase difference quadrature measurement due to asymmetry in the power incident on the two-sided cavity with  $\alpha_2 = 0.9\alpha_1$ . e) Effect of power asymmetry on quadrature measurements  $\theta = -\pi/4, -\pi/2$ .

the  $X_i$  quadratures from adding backaction induced noise to the system. Similar to the single-mode case, we see that the selection of the  $\theta$  which minimizes the backaction term is dependent on power ( $\alpha^2$ ). The noise metric  $N^2 \propto (x_E - (x_0 + \beta p_0/2))^2$  for the two-mode case may be expressed as

$$N^2 = \frac{1}{16\zeta^2} (\Delta Y + 2\zeta^2 \beta \Delta X + \Delta X \tan \theta)^2. \quad (17)$$

We now consider the effect of applying a squeezed two-mode vacuum to our two-sided cavity. For two-mode squeezed light, we see again that we have cross-correlation terms that are non-zero. The relevant vacuum expectation values comprising the amplitude difference and phase difference quadratures for two-mode squeezed light can be represented as,

$$\begin{aligned} \langle \Delta X^2 \rangle &= e^{2r} \cos^2 \phi + e^{-2r} \sin^2 \phi, \\ \langle \Delta Y^2 \rangle &= e^{-2r} \cos^2 \phi + e^{2r} \sin^2 \phi, \text{ and} \\ \langle \{\Delta X, \Delta Y\} \rangle &= (e^{-2r} - e^{2r}) \sin 2\phi, \end{aligned} \quad (18)$$

with the individual quadrature correlations represented as,

$$\begin{aligned} \langle X_1^2 \rangle &= \langle Y_1^2 \rangle = \langle X_2^2 \rangle = \langle Y_2^2 \rangle = \frac{1}{2} \cosh(2r), \\ \langle X_1 Y_1 \rangle &= \langle X_2 Y_2 \rangle = 0, \\ \langle X_1 Y_2 \rangle &= \langle X_2 Y_1 \rangle = \frac{1}{2} \sinh(2r) \sin(2\phi), \text{ and} \\ \langle X_1 X_2 \rangle &= -\langle Y_1 Y_2 \rangle = -\frac{1}{2} \sinh(2r) \cos(2\phi). \end{aligned} \quad (19)$$

From the above correlations we observe that the cross-terms can be made negative by choosing an appropriate squeezing angle and boosting the squeezing strength, to lower the noise floor for position measurements, as was the case for single-mode squeezed vacuum. In Figs. 2b-c we show that two-mode squeezed light is an alternative squeezing modality that may be used in position measurements providing the same noise floor with the same dependencies on the squeezing parameter  $r$ , squeezing angle  $\phi$ , and quadrature angle  $\theta$  as in the single-mode case discussed above. In the two-mode case, we are using



twice the amount of power compared to the single-mode case as both of the modes have equal amplitude. Thus, in the plot we notice that the optimal power requirement has reduced by a factor of half which is essentially equivalent to the single-mode case. We find that, at a squeezing angle of  $\phi = 0$ , squeezing reduces the power required to access the SQL for our system (see Fig. 2b). Similar to the single-mode case we see that for a squeezing angle of  $\phi = \pi/4$  and a non-zero squeezing strength the noise falls below the SQL near the original displacement amplitude  $\alpha$  due to the negative contribution from the cross-correlator term given by the aforementioned parameters. We globally minimize the noise by optimizing the quadrature angle  $\theta$ . The optimization gives us,  $\theta_{opt} \rightarrow -\tan^{-1}(2\zeta^2\beta)$  which is strongly dependent on power, similar to the single-mode case. This suggests that using this optimization at high power, we would measure the amplitude difference quadrature which is devoid of any signal, as in the single-mode case.

Two-mode squeezed light sources may have an asymmetry in the power of each mode. Additionally there may be mismatches in reflection coefficients for the two-sided cavity. As we will see, our toy model when driven by two-mode squeezed light or two coherent states, is robust to small amounts of asymmetries. If we account for a typical power asymmetry, we can modify the toy model as follows

$$U_{\text{meas}}U_{\text{free}}U_{\text{meas}} = e^{-ix_0(\zeta_1 X_1 - \zeta_2 X_2)} e^{-i\beta \frac{x_0^2}{2}} e^{-ix_0(\zeta_1 X_1 - \zeta_2 X_2)}. \quad (20)$$

To understand the impact of asymmetry we consider a specific example where the squeezing strength is  $r = 2$  as seen in Figs. 2d-e. We find numerically that the expected asymmetry of the modes with displacement amplitudes  $\alpha_1$  and  $\alpha_2$  should not exceed  $\alpha_2/\alpha_1 = 0.9$ , as seen in Fig. 2d. As our example illustrates, the squeezing and quadrature angles may be tuned to partially recover the noise floors of the symmetric case as seen in Fig. 2d-e. We expect that as  $r$  increases the amount of allowed asymmetry decreases.

### III. PRACTICAL DESIGN: SINGLE-SIDED CAVITY

With the intuition gained from our toy model, we investigate the benefits of squeezing in a single-sided optomechanical cavity as illustrated in Fig. 3a. The linearized interaction Hamiltonian for the cavity is

$$H_{\text{int}} = \hbar G x X, \quad (21)$$

where  $G$  is the optomechanical coupling strength in frequency per length units and  $x$  is the position of the moving mirror. The Hamiltonian  $H_{\text{tot}}$  that describes the optomechanical system in the rotating frame of the drive with the detuning  $\Delta$  is as follows,

$$\begin{aligned} H_{\text{tot}} &= H_{\text{cav}} + H_{\text{mech}} + H_{\text{int}} + H_{\text{bath}}, \\ H_{\text{cav}} &= -\hbar \Delta a^\dagger a, \text{ and} \\ H_{\text{mech}} &= \frac{1}{2} m \omega_m^2 x^2 + \frac{p^2}{2m}, \end{aligned} \quad (22)$$

where  $H_{\text{cav}}$ ,  $H_{\text{mech}}$ , and  $H_{\text{bath}}$  are the Hamiltonian terms for the optical cavity, the mechanical oscillator and the bath coupled to the system respectively. The parameters  $m$  and  $p$  are the mass and momentum of the moving mirror, respectively, in our system and  $\omega_m$  is the mechanical resonance frequency. On resonance with the drive,  $\Delta = 0$ , and the cavity Heisenberg-Langevin equations of motion are

$$\begin{aligned} \dot{X} &= -\frac{\kappa}{2} X + \sqrt{\kappa} X_{\text{in}}, \\ \dot{Y} &= -Gx - \frac{\kappa}{2} Y + \sqrt{\kappa} Y_{\text{in}}, \\ \dot{p} &= -\hbar G X - \gamma p + F_{\text{in}} - m \omega_m^2 x, \text{ and} \\ \dot{x} &= \frac{p}{m}, \end{aligned} \quad (23)$$

where  $\kappa$  is the cavity decay rate,  $X_{\text{in}}$  and  $Y_{\text{in}}$  are the quadratures input to the system,  $F_{\text{in}}$  is the external force acting on the resonator, and  $\gamma$  is the mechanical damping rate. The bath operators are expressed in terms of the input fields [48, 49]. The output quadratures are related to the input quadratures by the input-output relations

$$\begin{aligned} X_{\text{out}} &= X_{\text{in}} - \sqrt{\kappa} X, \text{ and} \\ Y_{\text{out}} &= Y_{\text{in}} - \sqrt{\kappa} Y. \end{aligned} \quad (24)$$

We determine  $X_{\text{out}}$  and  $Y_{\text{out}}$  in terms of the input fields. This analysis is done in the frequency domain by solving for all the variables  $X, Y, x, p$  in terms of the input fields  $X_{\text{in}}, Y_{\text{in}}$  and  $F_{\text{in}}$ . We then apply input-output relations to write down the expressions for  $X_{\text{out}}, Y_{\text{out}}$  as

$$\begin{aligned} X_{\text{out}} &= e^{i\phi_c} X_{\text{in}}, \text{ and} \\ Y_{\text{out}} &= e^{i\phi_c} Y_{\text{in}} + G \chi_c \chi_m [F_{\text{in}} - \hbar G \chi_c X_{\text{in}}]. \end{aligned} \quad (25)$$

The cavity response function  $\chi_c$ , the mechanical response function  $\chi_m$  and the cavity phase shift  $e^{i\phi_c}$  are,

$$\begin{aligned} \chi_c &= \frac{\sqrt{\kappa}}{-i\nu + \kappa/2}, \\ \chi_m &= \frac{-1}{m(\nu^2 - \omega_m^2 + i\gamma\nu)}, \text{ and} \\ e^{i\phi_c} &= \frac{-i\nu - \kappa/2}{-i\nu + \kappa/2}. \end{aligned} \quad (26)$$

We define the measurement quadrature output from the system as

$$X_\theta = Y_{\text{out}} \cos \theta + X_{\text{out}} \sin \theta. \quad (27)$$

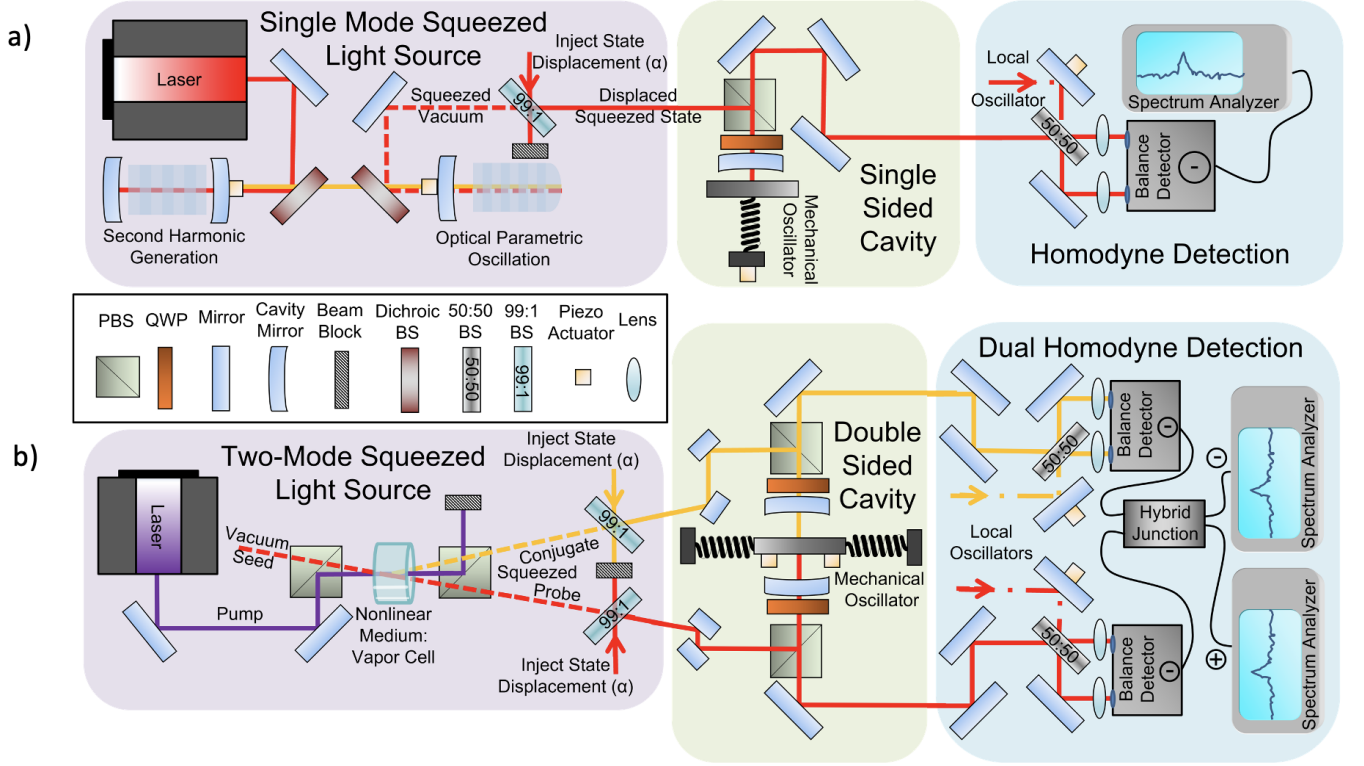


Figure 3. Experimental Vision: Schematics for a position measurement. a) A single-mode squeezed light source with displacement amplitude  $\alpha$  injected after squeezing, is used to interrogate an unfixed mirror in an optical cavity. The phase sensitive signal is read out with homodyne detection. b) A two-mode squeezed light source with  $\alpha$  injected onto the twin beams after squeezing, is used to interrogate an unfixed double-sided mirror in a double-sided optical cavity. The phase sensitive signal is read out with a joint measurement of the twin beams using dual homodyne detection.

By inspection of Eqs. 25 and 27 we obtain the estimator variable for the input force  $F_E$ , by dividing the output quadrature with the coefficient of the input force term  $G\chi_c\chi_m\cos\theta$ ,

$$F_E = \frac{X_\theta}{G\chi_c\chi_m\cos\theta} = \left[ \frac{e^{i\phi_c}\tan\theta}{G\chi_c\chi_m} - G\hbar\chi_c \right] X_{\text{in}} + \frac{e^{i\phi_c}Y_{\text{in}}}{G\chi_c\chi_m} + F_{\text{in}}. \quad (28)$$

We determine the two point correlation function  $\langle F_E(\nu)F_E(\nu') \rangle$  for  $F_E$  since  $\langle F_E(\nu)F_E(\nu') \rangle$  is proportional to the noise power spectral density (PSD)  $S_{FF}(\nu)$  as

$$\langle F_E(\nu)F_E(\nu') \rangle = S_{FF}(\nu)\delta(\nu + \nu'). \quad (29)$$

Understanding how to optimize the frequency-dependent power spectral density allows us to facilitate an intelligent search for a monochromatic or broadband signal. For a monochromatic signal, a frequency-dependent optimization of the PSD is required to obtain the maximum sensitivity. On the other hand, the optimized signal to noise ratio for a broadband signal corresponds to the noise PSD integrated over a bandwidth

of interest. For this case, an optimization over a broad frequency range would be necessary to obtain maximum sensitivity.

To consider the contributions to the noise, we focus on the quantity  $\langle F_E^2 \rangle$ . In the limit where the mechanical decay rate  $\gamma$  is much smaller than the other frequency scales ( $\gamma \ll \omega_m, \kappa$ ), the  $\gamma$ -dependent imaginary term of the cross-correlator may be neglected to obtain the following expression

$$\begin{aligned} \langle F_E^2 \rangle &= \left| \frac{e^{i\phi_c}\tan\theta}{G\chi_c\chi_m} - G\hbar\chi_c \right|^2 \langle X_{\text{in}}^2 \rangle + \left| \frac{1}{G\chi_c\chi_m} \right|^2 \langle Y_{\text{in}}^2 \rangle \\ &+ \left[ \hbar m(\omega_m^2 - \nu^2) + \frac{\tan\theta}{G^2|\chi_c|^2|\chi_m|^2} \right] \langle \{X_{\text{in}}, Y_{\text{in}}\} \rangle \\ &+ \langle F_{\text{in}}^2 \rangle. \end{aligned} \quad (30)$$

To optimally reduce the noise, we minimize  $\langle F_E^2 \rangle$  with respect to the quadrature angle  $\theta$  which reduces the back-action noise. Prior to minimizing the noise we fix the squeezing angle  $\phi$  to zero. This reveals the optimized quadrature angle

$$\theta_{\text{opt}} \rightarrow \tan^{-1} [\hbar G^2 m |\chi_c|^2 |\chi_m|^2 (\nu^2 - \omega_m^2)]. \quad (31)$$

By inspecting Eq. 31 we see that  $\theta_{\text{opt}}$  is strongly dependent on power ( $G^2 \propto \alpha^2$ ) and frequency. In the limit of high power and low frequency,  $\theta_{\text{opt}} = \pi/2$  which corresponds to measuring the amplitude quadrature  $X$  which is devoid of any signal from  $F_{\text{in}}$ . But in the high frequency limit  $\theta_{\text{opt}}$  approaches 0, allowing us to measure our signal at an optimally low noise floor. Our objective is to minimize the measurement-induced noise terms  $N(\nu)$  of  $\langle F_E^2 \rangle$ , so we only consider  $N(\nu)$  for the remainder of the section. While the thermal contribution to the noise may be reduced as discussed in [7], it is not the focus of this article. At the optimal quadrature angle and in the low  $\gamma$  limit, the measurement-induced noise  $N(\nu)$  for an arbitrary squeezing angle  $\phi$  simplifies to

$$N(\nu) = \frac{e^{-2r} \cos^2 \phi + e^{2r} \sin^2 \phi}{2G^2 |\chi_c|^2 |\chi_m|^2}. \quad (32)$$

Only the shot noise term is present in Eq. 32 since at  $\theta \rightarrow \theta_{\text{opt}}$  the backaction term of  $N(\nu)$  cancels out as  $\gamma \rightarrow 0$ . Here the optimal choice for squeezing angle is  $\phi = 0$ . With these parameters, the quantum noise is

$$\begin{aligned} N(\nu) &= \frac{e^{-2r}}{2G^2 |\chi_c|^2 |\chi_m|^2} \\ &\approx \frac{e^{-2r} m^2 (\kappa^2/4 + \nu^2)(\nu^2 - \omega^2)^2}{2G^2 \kappa}. \end{aligned} \quad (33)$$

As an alternative to the previous approach, by restricting ourselves to phase quadrature measurements, we may optimize  $N(\nu)$  with respect to power. A power optimization at  $\phi = 0$  leads to a target frequency-dependent coupling strength  $G$ ,

$$G(\nu) \rightarrow \frac{e^{-r}}{\sqrt{\hbar} |\chi_m(\nu)|^{1/2} |\chi_c(\nu)|}. \quad (34)$$

which demonstrates that when squeezing is present and the squeezing angle is zero the optimum power requirements to access the same noise floor are reduced, consistent with our toy model. Moreover, when we measure the phase quadrature while operating at the original optimized coupling strength as in the without squeezing case, a contribution to the total noise will be from the sum of the balanced shot noise and backaction noise terms. This sum is equivalent to the SQL. The additional contribution is from the cross-correlator term (the third term in Eq. 30). Careful selection of the squeezing angle  $\phi$ , will force the cross-correlator term to negatively contribute to the total noise expression, thus reducing the overall noise. Under these conditions, in the  $\gamma \rightarrow 0$  limit, the total measurement-induced noise is represented as

$$N(\nu) = \hbar m (\nu^2 - \omega_m^2) (\cosh 2r + \sinh 2r \sin 2\phi). \quad (35)$$

Equation 35 reveals that the measurement-induced noise is minimized by squeezing when the squeezing angle is tuned to  $\phi = -\pi/4$ .

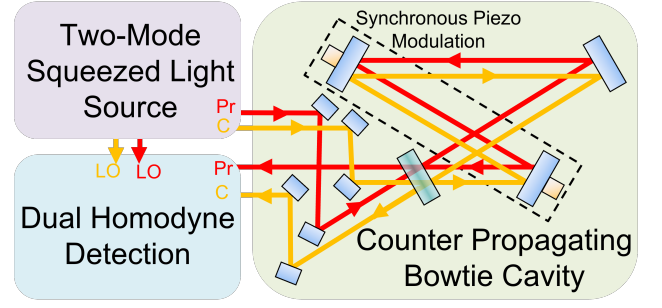


Figure 4. A momentum measurement where a bowtie cavity is probed by the counter-propagating modes of two-mode squeezed light. The modes enter the cavity through a beam splitter. The phase sensitive measurement interferes the squeezed modes with their local oscillators within dual homodyne detectors (as in Fig 3.b), enabling a momentum measurement imparted from a pair of synchronously modulated mirrors. The spatial modes may be overlapped by cross-polarizing the modes and using polarizing beamsplitters for injecting and collecting light from the cavity.

#### IV. COMBINING BACKACTION EVASION AND SQUEEZING

##### A. Continuous Momentum Measurement

In this section we consider a backaction evading model achieved by approaching a quantum non-demolition measurement of momentum, where we continuously monitor the momentum rather than the position of an optomechanical system using single-mode squeezed light. Momentum is effectively a QND variable while working in the free particle limit [26]. In our model, the light interacts directly with the momentum of the movable mirror in the system above rather than the position. Thus the interaction Hamiltonian is dependent on the momentum  $p$  of the system,

$$H_{\text{int}} = \hbar G' p X, \quad (36)$$

where  $G'$  is the optomechanical coupling strength in units of frequency over momentum. While this interaction cannot be directly generated by the single-sided optomechanical cavity discussed in the last section, there are some practical designs of optomechanical systems as described in the set-up of [6], as well as particular electromechanical couplings which essentially showcase the type of interaction described in Eq. 36. Furthermore, two-mode squeezed light can enable an experimental realization for a momentum measurement as described in Fig. 4 where the twin beams of two-mode squeezed light counter propagate through a bowtie cavity. We focus the remainder of this section on the benefits of a momentum based interaction and we do not consider its practical implementation any further. For the interaction Hamiltonian in Eq. 36, the Heisenberg-Langevin equations of motion are



$$\begin{aligned}
\dot{X} &= -\frac{\kappa}{2}X + \sqrt{\kappa}X_{\text{in}}, \\
\dot{Y} &= -G'p - \frac{\kappa}{2}Y + \sqrt{\kappa}Y_{\text{in}}, \\
\dot{p} &= -\gamma p + F_{\text{in}} - m\omega_m^2 x, \text{ and} \\
\dot{x} &= \frac{p}{m} + \hbar G'X.
\end{aligned} \tag{37}$$

The input and output quadratures for the optical fields are related by the input-output relations [48, 49]

$$\begin{aligned}
X_{\text{out}} &= X_{\text{in}} - \sqrt{\kappa}X, \text{ and} \\
Y_{\text{out}} &= Y_{\text{in}} - \sqrt{\kappa}Y.
\end{aligned} \tag{38}$$

We solve for the output quadratures in terms of the input quadratures as was done in Eq. 25 in the previous section. They are expressed as

$$\begin{aligned}
X_{\text{out}} &= e^{i\phi_c} X_{\text{in}}, \text{ and} \\
Y_{\text{out}} &= e^{i\phi_c} Y_{\text{in}} - iG'\chi_c\chi_m m\nu F_{\text{in}} \\
&\quad - \hbar m^2\omega_m^2 G'^2 \chi_c^2 \chi_m X_{\text{in}}.
\end{aligned} \tag{39}$$

As in the previous section, to estimate the force acting on the system, we divide a particular combination of the phase and amplitude quadrature as in Eq. 27 by the multiplicative factor for  $F_{\text{in}}$ , resulting in the force estimator variable

$$\begin{aligned}
F_E &= \frac{X_\theta}{-iG'\chi_c\chi_m m\nu \cos\theta}, \\
&= \left( \frac{ie^{i\phi_c} \tan\theta}{G'm\nu\chi_c\chi_m} - iG'\hbar\chi_c m \frac{\omega_m^2}{\nu} \right) X_{\text{in}} \\
&\quad + \frac{ie^{i\phi_c}}{G'm\nu\chi_c\chi_m} Y_{\text{in}} + F_{\text{in}}.
\end{aligned} \tag{40}$$

Our interest is in the contribution of the measurement-induced noise to the total noise PSD. To investigate the contributions to the noise PSD, we determine the two point correlation function of the estimator force variable as in the previous section

$$\begin{aligned}
\langle F_E^2 \rangle &= \left| \frac{ie^{i\phi_c} \tan\theta}{G'm\nu\chi_c\chi_m} - iG'\hbar\chi_c m \frac{\omega_m^2}{\nu} \right|^2 \langle X_{\text{in}}^2 \rangle \\
&\quad + \left| \frac{ie^{i\phi_c}}{G'm\nu\chi_c\chi_m} \right|^2 \langle Y_{\text{in}}^2 \rangle + \langle F_{\text{in}}^2 \rangle \\
&\quad \left[ \hbar m \frac{\omega_m^2}{\nu^2} (\omega_m^2 - \nu^2) + \frac{\tan\theta}{m^2\nu^2 G'^2 |\chi_c|^2 |\chi_m|^2} \right] \langle \{X_{\text{in}}, Y_{\text{in}}\} \rangle.
\end{aligned} \tag{41}$$

Note that there is no backaction noise in the limit where the mechanical frequency  $\omega_m \rightarrow 0$ , indicating the system is in the free particle limit. Fixing  $\phi = 0$ , from Eq. 41 we find the optimal quadrature angle which minimizes the noise

$$\theta_{\text{opt}} \rightarrow \tan^{-1} \left[ \hbar G'^2 m^3 \omega_m^2 |\chi_c|^2 |\chi_m|^2 (\nu^2 - \omega_m^2) \right]. \tag{42}$$

In the limit of  $\omega_m \rightarrow 0$ , the noise is minimized by measuring the phase quadrature corresponding to  $\theta_{\text{opt}} = 0$ . Under these conditions, the backaction term is canceled leaving only the shot noise term to contribute to the measurement-induced noise. Thus at  $\theta \rightarrow \theta_{\text{opt}}$ , in the low  $\gamma$  and free particle limit, the measurement-induced noise takes the form

$$N(\nu) = \frac{e^{-2r}\nu^2(\cos^2\phi + e^{4r}\sin^2\phi)}{2G'^2|\chi_c|^2}. \tag{43}$$

Since  $G'^2$  is proportional to power, an increase in the power will monotonically lower the noise floor. Squeezing can further minimize the measurement-induced noise for momentum sensing. By inspecting Eq. 43, we find that under these conditions, the optimal squeezing angle to lower the measurement-induced noise is  $\phi = 0$ . As in the case of position sensing, if we focus on the alternative approach where we only measure the phase quadrature, we can also optimize the measurement-induced noise with respect to power and obtain a target frequency-dependent coupling strength

$$G'(\nu) \rightarrow \frac{e^{-r}}{m\omega_m\sqrt{\hbar}|\chi_m(\nu)|^{1/2}|\chi_c(\nu)|}, \tag{44}$$

where the squeezing lowers the necessary power to attain a given noise floor. Using the original optimized power when squeezing is not present as an input into the total noise expression Eq. 41, we obtain the noise contributions from the SQL equivalent noise and the cross-correlator terms. Similar to the toy model and the position sensing scheme presented above, we see that by tuning the squeezing angle to  $\phi = -\pi/4$ , we force the cross-correlator term to be negative, thereby reducing the total noise. At the  $\gamma \rightarrow 0$  limit, the measurement-induced noise expression in this case can be represented as,

$$N(\nu) = \hbar m \frac{\omega_m^2}{\nu^2} (\nu^2 - \omega_m^2) (\cosh 2r + \sinh 2r \sin 2\phi). \tag{45}$$

## B. Comparisons

For position sensing, the coupling strength  $G$  scales as the frequency over the cavity length. For momentum sensing, the coupling constant  $G'$  scales as the frequency over momentum. For each technique, during measurement we coherently integrate the signal over the cavity lifetime. The momentum coupling strength  $G'$  is then related to  $G$  by the factor  $1/(m\kappa)$  where  $m$  is the mass of the mechanical sensor and  $\kappa$  is the cavity decay rate. We also choose  $1/\kappa$  as it is the natural scale in [6]. We begin by comparing the optimum quadrature angle that maximizes the signal-to-noise for the position and momentum sensing techniques. To compare the optimal quadrature

angles, the coupling strengths  $G$  and  $G'$  are chosen to produce the same power in both techniques. In Fig. 5a, we see that for a fixed value of  $G$  (corresponding to an input power of around 0.1 mW for a 1 cm cavity), the optimal quadrature for position sensing at low frequencies is the amplitude quadrature and at higher frequencies it is the phase quadrature. Whereas, under the same conditions, for momentum sensing we should optimally measure the phase quadrature across a broadband frequency spectrum. By fixing the frequency (here  $\nu = 10$  kHz), we find that in Fig. 5b, the optimal quadrature for position sensing deviates from the phase quadrature at much lower powers than in the momentum sensing case.

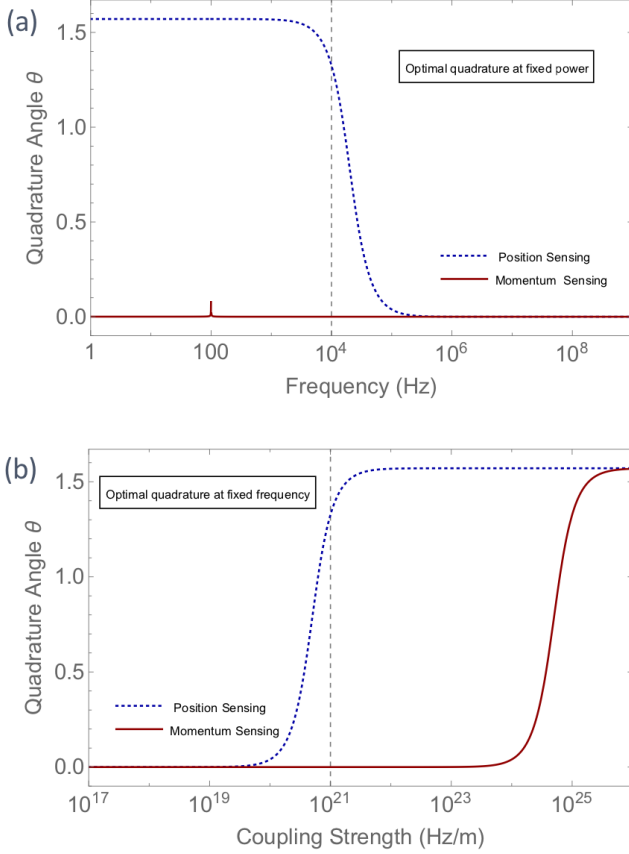


Figure 5. Optimal quadrature angle comparison between position sensing (Eq. 31) and momentum sensing (Eq. 42). a) Optimal quadrature angle plotted as a function of the frequency. The parameters used are the same as in Fig. 6 other than the coupling strength  $G$  which is fixed at  $10^{21}$  Hz/m and  $G' \rightarrow G/m\kappa$ . Position sensing has  $|\theta| \rightarrow \pi/2$  at lower frequency and  $|\theta| \rightarrow 0$  at higher frequency whereas for momentum sensing  $|\theta| \rightarrow 0$  for a broad spectrum. b) Optimal quadrature angle plotted as a function of the power. Here the frequency has been fixed at  $\nu \rightarrow 10$  kHz. We see that  $|\theta|$  starts to deviate from 0 at much lower power for position sensing than momentum sensing.

To compare the performance of the position and momentum sensing protocols, we must first distinguish be-

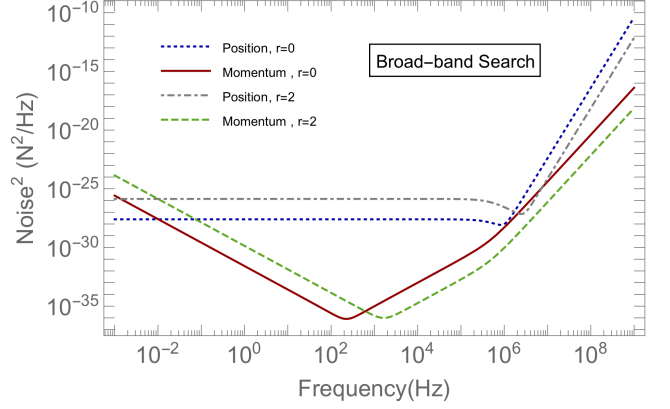


Figure 6. Broadband search strategy for position and momentum sensing. The phase quadrature noise is plotted for both sensing protocols while operating at the optimal power for position sensing with a 1 MHz target (using Eq. 34 at  $r=0$ ,  $\nu = 1$  MHz). The same power is used for the squeezed scenario. The optomechanical coupling strengths in these techniques are related by  $G' \rightarrow G/(m\kappa)$  with mechanical frequency  $\omega_m = 100$  Hz, cavity decay rate  $\kappa = 1$  MHz, mirror mass  $m = 1$  mg, damping rate  $\gamma = 0.1$  mHz, and squeezing angle  $\phi = 0$ . The noise for momentum sensing is lower than position sensing across a broad frequency range. At fixed power squeezing lowers the noise in the shot noise dominated region for both sensing protocols.

tween the relevant search strategies for specific signals. For dark matter detection, we distinguish between a monochromatic signal such as the coherent field generated by ultralight dark matter candidates [50] and broadband impulse signals expected in heavy dark matter candidates [7]. For the monochromatic signal, the exact frequency is unknown and consequently we consider narrow-band or resonant search strategies. For a heavy dark matter search including long-range interactions, the target frequency band is 1-10 MHz for the expected rapid impulse signal, where we consider a broadband search.

We begin our calculation for broadband search effectiveness by choosing the phase quadrature and optimally tuning the target laser power, corresponding to tuning the optomechanical coupling at a fixed target band center on the order of  $\sim 1$  MHz. We ensure that the coupling strengths for the momentum and the position sensing techniques are chosen such that for each technique the same target power is used during the broadband search. As represented in Fig. 6, we show the potential benefits of squeezing while operating at the same power. For the position sensing case, we are backaction limited at lower frequencies since we are operating at high input power  $P \sim 1$  W. We need this higher power when compared to the  $\nu = 10$  kHz case due to the much high frequency band-center. However, squeezing only provides a benefit at higher frequencies where we are shot noise limited. For momentum sensing, at frequencies below the mechanical resonance  $\omega_m$ , backaction dominates, so squeezing pro-

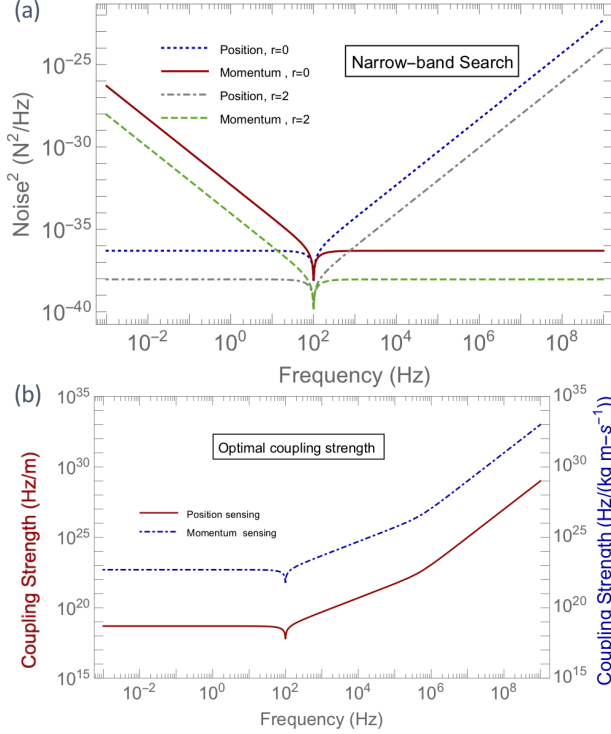


Figure 7. a) Narrow-band search strategy for position and momentum sensing. The noise is plotted for both techniques at the optimal power (Eqs. 34, 44 at  $r = 0$ ) and optimal quadrature angle (Eqs. 31, 42) for each frequency with a mechanical frequency  $\omega_m = 100$  Hz, cavity decay rate  $\kappa = 1$  MHz, sensor mass  $m = 1$  mg, damping rate  $\gamma = 0.1$  mHz, and squeezing angle  $\phi = 0$ . The optimal noise floor is lower in momentum sensing than position sensing when  $\nu > \omega_m$ . Squeezing at the same power lowers the noise floor. b) The optimal coupling strength dependence on frequency.

vides no improvement. Then backaction noise diminishes at higher frequencies than the mechanical resonance  $\omega_m$ , where we are shot noise limited. Hence, for momentum sensing, squeezing can significantly lower the noise in the regime of  $\nu > \omega_m$ . Additionally, we see that momentum sensing is more advantageous than position sensing for broadband detection as momentum sensing has a lower noise while operating at a fixed input power, especially for  $\nu > \omega_m$ .

We now describe the narrow-band search and its sensitivity as shown in Fig 7. Here we assume that the mechanical oscillator frequency is fixed. We begin the search by tuning the input power  $P$  at every frequency such that we set the noise floor to the SQL across the frequency spectrum. Simultaneously, at every frequency we select the optimal quadrature angle, in order to remove the backaction noise. We compare implementing our narrow-band search with ( $r = 2$ ) and without ( $r = 0$ ) using squeezed light, where the power used in each case is the same. Note that for the same power, squeezing lets

us achieve a lower noise floor in both position and the momentum sensing. By selecting the optimum quadrature the backaction term is eliminated and the remaining shot noise is reduced using squeezed light. For the position sensing case, we see that at frequencies below the mechanical frequency ( $\nu \ll \omega_m$ ), the noise is proportional to  $\hbar m \omega_m^2$  and is independent of frequency. The noise remaining constant across frequency in this scenario, is due to selecting an optimal  $G$ . In the same regime for momentum sensing, the noise goes as  $1/\nu^2$ . The opposite is true when  $\nu \gg \omega_m$  while operating at optimized powers, where the noise is flat for momentum sensing while the noise goes as  $\nu^2$  for position sensing. This characteristic can be attributed to the fact that the optimized noise in the momentum sensing technique is related to the optimized noise in the position sensing technique by a factor of  $\omega_m^2/\nu^2$ . Hence, for frequencies well above the mechanical frequency, we find the momentum sensing to be more advantageous than position sensing. With squeezing, the overall noise reduces in both cases by a constant factor dependent on the squeezing strength. While we see no particular improvement in the minimum noise attainable on resonance, we do see an improvement in the noise floor across off-resonance frequency regimes, for both the techniques through the narrow-band search strategy. This is in addition to the benefit from squeezing in achieving the same noise floor at a lower power.

## V. OUTLOOK

In this article, we have explored how to go beyond the SQL for optomechanical sensors using squeezing, backaction evasion, and QND techniques. From our toy model and our practical cavity example, we confirm that squeezing reduces the power needed to achieve a given noise floor for position sensing. We also examined a QND momentum sensing protocol using a momentum coupling model, which shows equal benefits from squeezing in terms of power requirements. Critically, in the momentum sensing model at the free particle limit, as the backaction term goes to zero, we need to only measure the phase quadrature. Specifically, there is neither frequency nor power dependence to the optimal quadrature angle, thereby reducing the technical challenges of using squeezing in comparison to squeezed position sensing.

We have also explored search strategies for monochromatic and broadband signals. For broadband signals we determined that our momentum sensing model provides us with an improved noise floor over a broad frequency range. In both techniques, the noise floor is lowered in the shot noise dominated regime using squeezed light at the same operating power. For monochromatic signals, in the low frequency regime position sensing outperforms momentum sensing and at the high frequency regime we see the opposite. Furthermore, by using squeezed light we can achieve a lower noise floor for both protocols by optimally tuning the quadrature angle and power.

The quantum-enhanced sensing techniques presented in this article are especially useful in the context of direct dark matter detection as previously discussed. Our techniques may also be used in impulse metrology experiments such as sensing the collisions from background gas particles. In order to practically implement the momentum sensing technique, we can use specific designs of optomechanical system or an electrical system for readout. The electrical alternative is part of an ongoing work by some of the authors here and will be explored in a separate manuscript. The analysis in this article provides the key insight that we may reduce the noise floor for an optomechanical sensor by combining backaction evasion through a momentum measurement and squeezing. Moreover, the momentum sensing approach has advantages in terms of bandwidth and a reduction in technical noise caused by power fluctuations. We foresee that deploying these techniques would aid in reducing the measurement-induced noise floor for optomechanical sensors and would pave the way for extremely sensitive impulse detections.

## VI. ACKNOWLEDGEMENT

We thank Peter Shawhan, Daniel Carney, Jon Kujummen, and Alberto Marino for helpful conversation. SG is supported by the Physics Frontier Center at the Joint Quantum Institute, which is funded through the National Science Foundation (Award no. 1430094). This work was performed in part at Oak Ridge National Laboratory, operated by UT-Battelle for the U.S. Department of Energy under contract no. DE-AC05-00OR22725. RP and CM were supported by the U.S. DOE, Office of Science, National Quantum Information Science Research Centers, Quantum Science Center and by the U.S. DOE Office of Science, Office of High Energy Physics. Postdoc support for SH and MF was provided by the DOE Office of Science, Office of High Energy Physics, and for MF by the U.S. DOE Office of Science, National Quantum Information Science Research Centers, Quantum Science Center.

## Appendix A

We consider continuously monitoring the position of a single-sided optomechanical system, comprising a fixed mirror and a pendulous mirror. We probe the system with either classical or single-mode squeezed light as seen in the schematic diagram of Fig. 1a and the proposed experimental implementation of Fig. 3a. A typical single-sided optomechanical system, in the linearized domain where the operators for the fields in the cavity have been displaced by a large displacement amplitude  $\alpha$  relative to the quadrature fluctuations [48, 51], has an optomechanical interaction described by the Hamiltonian

$$\begin{aligned} H_{\text{int}} &= \hbar G x X, \\ &= \hbar g_o \alpha x X. \end{aligned} \quad (\text{A1})$$

Here,  $x$  is the position of the system,  $X$  is the amplitude quadrature of light,  $g_o$  is the single-photon optomechanical coupling strength in frequency per length units and  $G$  is the optomechanical coupling strength enhanced by the displacement amplitude  $\alpha$ . In the linearized domain the displacement amplitude is proportional to the square root of the power of the probing light.

For the Hamiltonian,  $\alpha$  sets the phase reference for our system and is assumed to be real ( $\alpha \in \mathbb{R}$ ).

By monitoring the phase of the light reflected from the system, we can determine the system position and the source of the backaction in the measurement.

For a squeezed vacuum this interaction Hamiltonian holds when the photons from the displacement amplitude  $n$  are much greater than the squeezed vacuum  $n_{\text{vac}}$ . For the unitary evolution of our toy models the interaction scales linearly by the factor  $\zeta = \alpha\mu$ . Here the displacement amplitude  $\alpha$  is amplified by the factor  $\mu = gt_{\text{int}} \approx g/\kappa$  where  $g$  is the single-photon optomechanical coupling strength in frequency,  $t_{\text{int}}$  is the interaction time and  $\kappa$  is the cavity linewidth. For an optomechanical cavity the intracavity photons are related to the displacement amplitude driving it by  $\alpha = \sqrt{n}$ . For typical single-photon optomechanical coupling strengths  $g < 1$  kHz and cavity linewidths  $\kappa > 10$  MHz [45, 46]. As an example, near the minimum displacement amplitude we drive the toy model with ( $\mu\alpha = 0.02$ ), the intracavity photon number is  $n = 4000$ . The number of photons in a squeezed vacuum state is  $\langle n_{\text{vac}} \rangle = \sinh^2 r$ . Hence the photons generated by the displacement amplitude exceed the vacuum photon number  $n_{\text{vac}}$  (with  $r=2$ ) fluctuations by orders of magnitude so we may neglect the contribution to of  $n_{\text{vac}}$  to the amplitude displacement.

---

[1] Carlton M Caves, Kip S Thorne, Ronald WP Drever, Vernon D Sandberg, and Mark Zimmermann. On the measurement of a weak classical force coupled to a

quantum-mechanical oscillator. i. issues of principle. *Reviews of Modern Physics*, 52(2):341, 1980.

[2] SP Vyatchanin and EA Zubova. Quantum variation mea-

- surement of a force. *Physics letters A*, 201(4):269–274, 1995.
- [3] Vladimir B Braginsky, Mikhail L Gorodetsky, Farid Ya Khalili, Andrey B Matsko, Kip S Thorne, and Sergey P Vyatchanin. Noise in gravitational-wave detectors and other classical-force measurements is not influenced by test-mass quantization. *Physical Review D*, 67(8):082001, 2003.
  - [4] Sydney Schreppler, Nicolas Spethmann, Nathan Brahms, Thierry Botter, Maryrose Barrios, and Dan M Stamper-Kurn. Optically measuring force near the standard quantum limit. *Science*, 344(6191):1486–1489, 2014.
  - [5] LF Buchmann, S Schreppler, J Kohler, N Spethmann, and DM Stamper-Kurn. Complex squeezing and force measurement beyond the standard quantum limit. *Physical review letters*, 117(3):030801, 2016.
  - [6] Sohritri Ghosh, Daniel Carney, Peter Shawhan, and Jacob M Taylor. Backaction-evading impulse measurement with mechanical quantum sensors. *Physical Review A*, 102(2):023525, 2020.
  - [7] Daniel Carney, Sohritri Ghosh, Gordan Krnjaic, and Jacob M Taylor. Proposal for gravitational direct detection of dark matter. *Physical Review D*, 102(7):072003, 2020.
  - [8] Daniel Carney, Gordan Krnjaic, David C Moore, Cindy A Regal, Gadi Afek, Sunil Bhawe, Benjamin Brubaker, Thomas Corbitt, Jonathan Cripe, Nicole Crisosto, et al. Mechanical quantum sensing in the search for dark matter. *Quantum Science and Technology*, 6(2):024002, 2021.
  - [9] Alaina Attanasio, Sunil A Bhawe, Carlos Blanco, Daniel Carney, Marcel Demarteau, Bahaa Elshimy, Michael Febbraro, Matthew A Feldman, Sohritri Ghosh, Abby Hickin, et al. Snowmass 2021 white paper: The windchime project. *arXiv preprint arXiv:2203.07242*, 2022.
  - [10] JK Fremerey. Spinning rotor vacuum gauges. *Vacuum*, 32(10-11):685–690, 1982.
  - [11] J Patrick Looney, Joel E Harrington, Kermit C Smyth, Thomas R O’Brian, and Thomas B Lucatorto. Measurement of co pressures in the ultrahigh vacuum regime using resonance-enhanced multiphoton-ionization time-of-flight mass spectroscopy. *Journal of Vacuum Science & Technology A: Vacuum, Surfaces, and Films*, 11(6):3111–3120, 1993.
  - [12] T Arpornthip, CA Sackett, and KJ Hughes. Vacuum-pressure measurement using a magneto-optical trap. *Physical Review A*, 85(3):033420, 2012.
  - [13] VB Makhalov, KA Martinyanov, and AV Turlapov. Primary vacuum measurement based on an ultracold gas in a shallow optical dipole trap. *Metrologia*, 53(6):1287, 2016.
  - [14] Stephen Eckel, Daniel S Barker, James A Fedchak, Nikolai N Klimov, Eric Norrgard, Julia Scherschligt, Constantinos Makrides, and Eite Tiesinga. Challenges to miniaturizing cold atom technology for deployable vacuum metrology. *Metrologia*, 55(5):S182, 2018.
  - [15] Mankei Tsang and Carlton M Caves. Coherent quantum-noise cancellation for optomechanical sensors. *Physical review letters*, 105(12):123601, 2010.
  - [16] John Melcher, Julian Stirling, Felipe Guzmán Cervantes, Jon R Pratt, and Gordon A Shaw. A self-calibrating optomechanical force sensor with femtonewton resolution. *Applied Physics Letters*, 105(23):233109, 2014.
  - [17] Xunnong Xu and Jacob M Taylor. Squeezing in a coupled two-mode optomechanical system for force sensing below the standard quantum limit. *Physical Review A*, 90(4):043848, 2014.
  - [18] Maximilian H Wimmer, Daniel Steinmeyer, Klemens Hammerer, and Michèle Heurs. Coherent cancellation of backaction noise in optomechanical force measurements. *Physical Review A*, 89(5):053836, 2014.
  - [19] Xunnong Xu and Jacob M. Taylor. Squeezing in a coupled two-mode optomechanical system for force sensing below the standard quantum limit. *Phys. Rev. A*, 90:043848, Oct 2014.
  - [20] David Mason, Junxin Chen, Massimiliano Rossi, Yeghishe Tsaturyan, and Albert Schliesser. Continuous force and displacement measurement below the standard quantum limit. *Nature Physics*, 15(8):745–749, 2019.
  - [21] RC Pooser, Nicholas Savino, Emma Batson, JL Beckey, J Garcia, and BJ Lawrie. Truncated nonlinear interferometry for quantum-enhanced atomic force microscopy. *Physical Review Letters*, 124(23):230504, 2020.
  - [22] Raphael C Pooser and Benjamin Lawrie. Ultrasensitive measurement of microcantilever displacement below the shot-noise limit. *Optica*, 2(5):393–399, 2015.
  - [23] M e Tse, Haocun Yu, Nutsinee Kijbunchoo, A Fernandez-Galiana, P Dupej, L Barsotti, CD Blair, DD Brown, SE Dwyer, A Effler, et al. Quantum-enhanced advanced ligo detectors in the era of gravitational-wave astronomy. *Physical Review Letters*, 123(23):231107, 2019.
  - [24] Chang-Woo Lee, Jae Hoon Lee, and Hyojun Seok. Squeezed-light-driven force detection with an optomechanical cavity in a mach–zehnder interferometer. *Scientific Reports*, 10(1):1–16, 2020.
  - [25] Ali Motazedifard, F Bemani, MH Naderi, R Roknizadeh, and D Vitali. Force sensing based on coherent quantum noise cancellation in a hybrid optomechanical cavity with squeezed-vacuum injection. *New Journal of Physics*, 18(7):073040, 2016.
  - [26] Vladimir B Braginsky, Yuri I Vorontsov, and Kip S Thorne. Quantum nondemolition measurements. *Science*, 209(4456):547–557, 1980.
  - [27] Philippe Grangier, Juan Ariel Levenson, and Jean-Philippe Poizat. Quantum non-demolition measurements in optics. *Nature*, 396(6711):537–542, 1998.
  - [28] Aashish A Clerk, Florian Marquardt, and K Jacobs. Back-action evasion and squeezing of a mechanical resonator using a cavity detector. *New Journal of Physics*, 10(9):095010, 2008.
  - [29] MD Levenson, RM Shelby, M Reid, and DF Walls. Quantum nondemolition detection of optical quadrature amplitudes. *Physical review letters*, 57(20):2473, 1986.
  - [30] A La Porta, RE Slusher, and B Yurke. Back-action evading measurements of an optical field using parametric down conversion. *Physical review letters*, 62(1):28, 1989.
  - [31] JB Hertzberg, T Rocheleau, T Ndikum, M Savva, Aashish A Clerk, and KC Schwab. Back-action-evading measurements of nanomechanical motion. *Nature Physics*, 6(3):213–217, 2010.
  - [32] MR Vanner, J Hofer, GD Cole, and M Aspelmeyer. Cooling-by-measurement and mechanical state tomography via pulsed optomechanics. *Nature communications*, 4(1):1–8, 2013.
  - [33] Itay Shomroni, Liu Qiu, Daniel Malz, Andreas Nunnenkamp, and Tobias J Kippenberg. Optical backaction-evading measurement of a mechanical oscillator. *Nature communications*, 10(1):1–7, 2019.
  - [34] Yulong Liu, Jingwei Zhou, Laure Mercier de Lépinay, and Mika A Sillanpää. Quantum backaction evading measurements of a silicon nitride membrane resonator. *arXiv*



- preprint *arXiv:2201.11041*, 2022.
- [35] Sergey P Vyatchanin and Andrey B Matsko. Broadband quantum back action evading measurements of a resonant force. *Physics Letters A*, 424:127849, 2022.
  - [36] Jonathan Cripe, Torrey Cullen, Yanbei Chen, Paula Heu, David Follman, Garrett D Cole, and Thomas Corbitt. Quantum backaction cancellation in the audio band. *Physical Review X*, 10(3):031065, 2020.
  - [37] Min Jet Yap, Jonathan Cripe, Georgia L Mansell, Terry G McRae, Robert L Ward, Bram JJ Slagmolen, Paula Heu, David Follman, Garrett D Cole, Thomas Corbitt, et al. Broadband reduction of quantum radiation pressure noise via squeezed light injection. *Nature Photonics*, 14(1):19–23, 2020.
  - [38] Chuming Wang, Chunong Zhao, Xiang Li, Enping Zhou, Haixing Miao, Yanbei Chen, and Yiqiu Ma. Boosting the sensitivity of high frequency gravitational wave detectors by pt-symmetry. *arXiv preprint arXiv:2206.13224*, 2022.
  - [39] Xiang Li, Maxim Goryachev, Yiqiu Ma, Michael E Tobar, Chunong Zhao, Rana X Adhikari, and Yanbei Chen. Broadband sensitivity improvement via coherent quantum feedback with pt symmetry. *arXiv preprint arXiv:2012.00836*, 2020.
  - [40] Tuvia Gefen, Rajashik Tarafder, Rana X Adhikari, and Yanbei Chen. Quantum precision limits of displacement noise free interferometers. *arXiv preprint arXiv:2209.02998*, 2022.
  - [41] Huaixiu Zheng, Matti Silveri, RT Brierley, SM Girvin, and KW Lehnert. Accelerating dark-matter axion searches with quantum measurement technology. *arXiv preprint arXiv:1607.02529*, 2016.
  - [42] M Malnou, DA Palken, BM Brubaker, Leila R Vale, Gene C Hilton, and KW Lehnert. Squeezed vacuum used to accelerate the search for a weak classical signal. *Physical Review X*, 9(2):021023, 2019.
  - [43] Akash V Dixit, Srivatsan Chakram, Kevin He, Ankur Agrawal, Ravi K Naik, David I Schuster, and Aaron Chou. Searching for dark matter with a superconducting qubit. *Physical review letters*, 126(14):141302, 2021.
  - [44] Anthony J Brady, Christina Gao, Roni Harnik, Zhen Liu, Zheshen Zhang, and Quntao Zhuang. Entangled sensor-networks for dark-matter searches. *arXiv preprint arXiv:2203.05375*, 2022.
  - [45] D.J. Wilson, V. Sudhir, N. Piro, R. Schilling, A. Ghadimi, and T. J. Kippenberg. Measurement-based control of a mechanical oscillator at its thermal decoherence rate. *Nature*, 524:325–329, 2015.
  - [46] Massimiliano Rossi, David Mason, Junxin Chen, Yeghishe Tsaturyan, and Albert Schliesser. Measurement-based quantum control of mechanical motion. *Nature*, 563:53–58, 2018.
  - [47] Rodney Loudon and Peter L Knight. Squeezed light. *Journal of modern optics*, 34(6-7):709–759, 1987.
  - [48] A. A. Clerk, M. H. Devoret, S. M. Girvin, Florian Marquardt, and R. J. Schoelkopf. Introduction to quantum noise, measurement, and amplification. *Rev. Mod. Phys.*, 82:1155–1208, Apr 2010.
  - [49] CW Gardiner and MJ Collett. Input and output in damped quantum systems: Quantum stochastic differential equations and the master equation. *Physical Review A*, 31(6):3761, 1985.
  - [50] Daniel Carney, Anson Hook, Zhen Liu, Jacob M Taylor, and Yue Zhao. Ultralight dark matter detection with mechanical quantum sensors. *New Journal of Physics*, 23(2):023041, 2021.
  - [51] Markus Aspelmeyer, Tobias J Kippenberg, and Florian Marquardt. Cavity optomechanics. *Reviews of Modern Physics*, 86(4):1391, 2014.